Journal for ImmunoTherapy of Cancer

Necroptosis-driving genes *RIPK1, RIPK3* and *MLKL-p* are associated with intratumoral CD3$^+$ and CD8$^+$ T cell density and predict prognosis in hepatocellular carcinoma

Lorenzo Nicolè ,[1,2] Tiziana Sanavia ,[3] Rocco Cappellesso,[4] Valeria Maffeis,[5] Jun Akiba,[6] Akihiko Kawahara,[6] Yoshiki Naito,[6] Claudia Maria Radu,[7] Paolo Simioni,[7] Davide Serafin,[8] Giuliana Cortese,[8] Maria Guido,[1,5] Giacomo Zanus,[9,10] Hirohisa Yano,[11] Ambrogio Fassina[1]

To cite: Nicolè L, Sanavia T, Cappellesso R, *et al*. Necroptosis-driving genes *RIPK1, RIPK3* and *MLKL-p* are associated with intratumoral CD3$^+$ and CD8$^+$ T cell density and predict prognosis in hepatocellular carcinoma. *Journal for ImmunoTherapy of Cancer* 2022;**10**:e004031. doi:10.1136/jitc-2021-004031

► Additional supplemental material is published online only. To view, please visit the journal online (http://dx.doi.org/10.1136/jitc-2021-004031).

LN and TS contributed equally.

LN and TS are joint first authors.

Accepted 21 January 2022

For numbered affiliations see end of article.

Correspondence to
Professor Ambrogio Fassina; ambrogio.fassina@unipd.it

ABSTRACT

Background Hepatocellular carcinoma (HCC) is a highly lethal cancer and the second leading cause of cancer-related deaths worldwide. As demonstrated in other solid neoplasms and HCC, infiltrating CD8$^+$ T cells seem to be related to a better prognosis, but the mechanisms affecting the immune landscape in HCC are still mostly unknown. Necroptosis is a programmed, caspase-independent cell death that, unlike apoptosis, evokes immune response by releasing damage-associated molecular factors. However, in HCC, the relationship between the necroptotic machinery and the tumor-infiltrating lymphocytes has not been fully investigated so far.

Methods We investigated the association between the main necroptosis-related genes, that is, *RIPK1, RIPK3, MLKL-p*, and CD3$^+$/CD8$^+$ tumor-infiltrating T cell by RNA-seq data analysis in 371 patients with primary HCC from The Cancer Genome Atlas and then by immunohistochemistry in two independent cohorts of HCC patients from Italy (82) and Japan (86).

Results Our findings highlighted the immunogenetic role of necroptosis and its potential prognostic role in HCC: RIPK1, RIPK3 and MLKL-p were found significantly associated with intratumoral CD3$^+$ and CD8$^+$ T cells. In addition, multivariate survival analysis showed that the expression of RIPK1, RIPK3 and MLKL-p was associated with better overall survival in the two independent cohorts.

Conclusions Our results confirmed the immunogenetic properties of necroptosis (NCP) in human HCC, showing that tumor-infiltrating lymphocytes (TILs) and, specifically, CD8+ T cells accumulate in tumors with higher expression of the necroptosis-related genes. These results suggest the importance of further studies to better assess the specific composition, as well as the functional features of the immune environment associated with a necroptotic signature in order to explore new possible diagnostic and immunotherapeutic scenarios.

INTRODUCTION

Hepatocellular carcinoma (HCC) is the second leading cause of cancer-related human deaths.[1] Most HCCs arise in cirrhotic liver, related to chronic viral infections by hepatitis C virus or hepatitis B virus, alcohol abuse, aflatoxin exposure or metabolic or autoimmune liver diseases.[2] Since most HCCs are diagnosed in an advanced stage, gold-standard treatments like tumor resection, local radiofrequency ablation and, in selected cases, liver transplantation[3] are ineffective, with a high rate of recurrence and low survival.[2] Moreover, HCC clinical outcomes can be different in patients with the same tumor, node and metastasis (TNM) stage, and effective prognostic markers are still largely limited so far.

The role of the tumor microenvironment (TME) in promoting tumor aggressiveness has been well established in the last years,[4] but little is known about the complex and highly dynamic network driving immune and stromal cell interactions within the tumor. Features such as entity, degree, and spatial distribution of infiltrating T cells can be used to obtain a more accurate stratification of the patients, according to phenotype, prognosis, and treatment susceptibility.[5,6] The prognostic role of the intratumoral CD3$^+$ and CD8$^+$ T cells has been already described in association with the standard TNM staging system,[7,8] but TME intrinsic features have been poorly investigated in HCC so far.

Programmed cell death is known to have a great impact in featuring the TME ecosystem.[9] Transformed hepatocytes can die by different types of regulated cell death pathways, and the most known are apoptosis and necroptosis (NCP).[10] In contrast to apoptosis, which typically limits inflammation, NCP induces membrane destabilization followed

by cellular swelling and lysis, with consequent dissemination of intracellular constituents. NCP pathway is activated by the co-presence of inhibited caspase 8 and the receptor-interacting serine/threonine-protein kinase 1 (RIPK1), which promotes NCP through the recruitment and the activation of the receptor-interacting serine/threonine-protein kinase 3 (RIPK3). Activated RIPK3 promotes the activation of the mixed lineage kinase domain-like protein (MLKL), which migrates to the cell membrane and then oligomerizes to form a channel-like structure promoting the membrane destabilization and disruption. Disseminated cellular elements are identified as damage-associated molecular patterns (DAMPs).[11] DAMPs floating within the extracellular space are then recognized by immature antigen-presenting cells that may engage adaptive immunity, boosting tumor surveillance through the cytotoxic $CD8^+$ T cells activation.[12]

In this study, we assessed the impact of NCP in influencing the lymphocyte landscape of HCC. We first evaluated the association between the expression of the genes involved in NCP and the $CD8^+$ infiltration using RNA-seq data of 371 patients with primary HCC from The Cancer Genome Atlas (TCGA). Second, in line with the results obtained from the computational analysis, we evaluated the expression of the main NCP-associated proteins (i.e., RIPK1, RIPK3 and MLKL-p) by immunohistochemistry (IHC) in two independent cohorts of 86 Italian and 82 Japanese HCC patients, suggesting a necroptosis core score (NCS) to quantify the expression of the NCP machinery in the tissue samples. Associations between NCS and the tumor-infiltrating lymphocytes $CD3^+$ and $CD8^+$ were then assessed. Finally, we retrospectively investigated the prognostic impact of NCS and the intratumoral $CD3^+$ and $CD8^+$ T cells infiltrate. To our knowledge, this is the most extensive study exploring the necroptotic machinery in HCC from different cohorts of patients.

MATERIALS AND METHODS

Bioinformatics and statistical analysis of TCGA data

We initially investigated to which extent the NCP pathway is correlated to $CD8^+$ T cell infiltration in public HCC data, following the pipeline described in figure 1A. Three hundred and seventy-one primary solid tumors with available bulk RNA-seq expression data were considered from the TCGA Liver Hepatocellular Carcinoma (LIHC) project.[13] Ninety-one primary solid tumors were filtered out to exclude cases with pharmaceutical or radiation treatments before surgery, cases with a history of neoadjuvant treatments or other malignancies and cases with residual tumor. Clinical data of the selected patients are displayed in table 1. From the complex mixture of cells in HCC RNA-seq bulk samples, immune cell infiltration was estimated through a consensus score built from three popular deconvolution algorithms used to estimate the proportion of specific cell populations ($CD8^+$ T cells in our case) from gene expression data (methods details in online supplemental file 1 and figure S1; estimations and final consensus ranking available in online supplemental table 1). Considering the 25th and 75th percentiles of the consensus ranking, 70+70 samples at low and high TILs infiltration were isolated.

Logistic regression was first applied to each gene belonging to the NCP pathway (n=163, annotations from KEGG database[14]) to test its association with $CD8^+$ T cell infiltration. Then, considering the interaction network of the NCP pathway, multivariate logistic regression was applied to all the groups of genes belonging to a common (shortest) path of interactions in the network including at least one gene previously found significantly associated with $CD8^+$ infiltration. In both analyses, tumor purity was considered as confounder in the models (data from Aran *et al*[15]). Likelihood ratio test was applied to test the significance in each model, considering Benjamini-Hochberg adjusted p-values <0.05 as significant. For the multivariate analysis, p-values <0.05 in the Wald tests of all the estimated coefficients characterizing the contribution of the expression levels of each gene in the path were also required for the statistical significance. Analyses were performed with R (V.4.0.3, https://www.R-project.org/).

Patients and specimens description

Two cohorts of 82 Italian and 86 Japanese patients that underwent surgical resection for primary HCC between 2008 and 2012 were considered (figure 2A and table 2). Representative formalin-fixed and paraffin-embedded (FFPE) HCC specimens for each patient were retrieved from the archives of the Pathology Unit of the University of Padova and of the Department of Diagnostic Pathology of Kurume University Hospital.

The following inclusion criteria were considered: (A) European/Asian ethnicity with available follow-up data; (B) histologically complete resection (R0); (C) known etiology; and (D) availability of biological material.

All cases were reviewed to confirm the histological diagnosis following the WHO classification of tumors.[16] All the experimental procedures were performed according to the 1964 Helsinki declaration and its later amendments, following the REporting recommendations for tumor MARKer prognostic studies guidelines.[17]

IHC and immunofluorescence microscopy (IF)

IHC was performed following the manufacturer's suggestions on 4 µm sections from the most representative FFPE samples as previously described,[18] using primary antibodies against RIPK1, RIPK3 and MLKL-p (antibody specifications are displayed in table S1 in online supplemental file 1). Under the optical microscope, cytoplasmic or membrane immunostaining for RIPK1, RIPK3, and MLKL-p were assessed as percentage of positive cancer cells and then stratified into four groups (figure 2B, from A1 to C4): 0 (expression <5%); 1+ (expression 5%–25%); 2+ (expression 25%–65%); and 3+ (expression >65%). A score for each marker was performed by two pathologists (LN and VM; concordance between observers is shown in figure S2 in online supplemental file 1). Representative

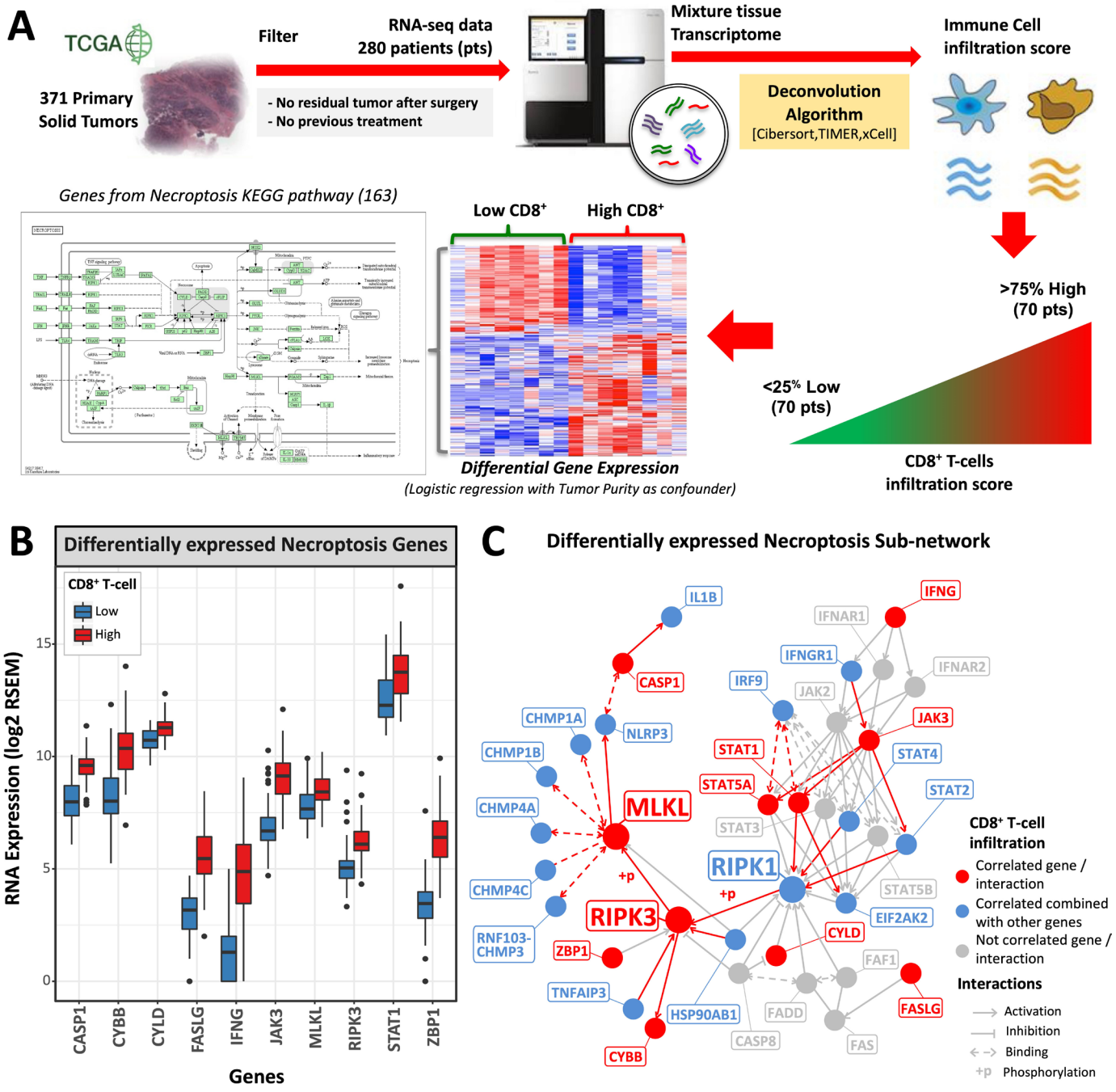

Figure 1 Association analysis between CD8+ infiltration and transcriptional expression of Necroptosis genes in TCGA data. (A) Bioinformatic pipeline by estimating the CD8+ infiltration score using deconvolution methods and then considering the extreme quartiles to define patients at low and high immune infiltration. This score was then applied as a binary dependent variable for the logistic regression model in order to select, among the genes belonging to the necroptosis pathway from KEGG, those resulting significantly associated with the immune infiltration. (B) Boxplot of the differential expression at low and high CD8+ infiltration of the necroptosis genes selected by the univariate logistic regression, using tumor purity as confounder. (C) Subnetwork of the necroptosis pathway including all the genes selected by both univariate (red nodes) and multivariate (blue nodes) logistic regression. Red edges show the paths/combinations of the genes significantly associated with the immune infiltration in the multivariate regression (see table S1 in online supplemental file 1 for the complete list). Abbreviations: TCGA, The Cancer Genome Atlas.

immunostaining for each necroptotic marker and its role in the pathway are displayed in figure 3. To evaluate the overall expression of NCP in each case, we calculated a NCS ranging from 0 to 9, defined by the sum of the single scores of each marker. NCS was used to stratify patients in three groups according to the level of activated NCP (low: NCS ranging from 0 to 3; intermediate: NCS ranging from 4 to 6; and high: NCS ranging from 7 to 9). Infiltrating lymphocytes were stained with CD3+ and CD8+ antibodies and then automatically detected in

Table 1 Demographic and pathological data of the 280 TCGA-LIHC patients

Patient/tumor characteristics	% (n)
Age (years)	
Mean (SD)	59 (13)
Sex	
Female	32 (90)
Male	68 (190)
Ethnicity	
Caucasian	43 (121)
Other (90% Asian)	54 (150)
Missing	3.2 (9)
Child-Pugh	
A	62% (173)
B	6.8% (19)
C	0.36% (1)
Missing	31% (87)
Stage (AJCC)	
Stage I–II	71 (198)
Stage III–IV	24 (67)
Missing	5.4 (15)
Grade	
G1–G2	59 (166)
G3–G4	40 (113)
Missing	0.36 (1)
Vascular invasion	
Macro	3.9 (11)
Micro	25 (71)
None	55 (155)
Missing	15 (43)
5-year recurrence	
No	41 (116)
Yes	48 (134)
Missing	11 (30)
5-years survival	
Death	34 (94)
Alive	66 (186)

AJCC, American Joint Committee on Cancer; TCGA, The Cancer Genome Atlas.

tumorous tissues using a custom-made algorithm created with Visiopharm software, V.4.5.6.5 (Visiopharm, Hoersholm, Denmark),[19] as described in online supplemental file 1. Slices from Italian and Japanese cohorts were set up under the same experimental conditions.

IF on FFPE sections of a representative case was performed to confirm colocalization of the necroptotic proteins in tumor cells. The selected sample was labeled by a sequential double stain to analyze the simultaneous expression of the antigens RIPK3-RIPK1 and MLKL-RIPK1, and then examined by Leica DMI6000CS fluorescence microscope (Leica Microsystem, Wetzlar, Germany). Sections were analyzed with differential interference contrast (DIC) and fluorescence objectives. Protocol details are described in online supplemental file 1.

Statistical analysis in Italian and Japanese cohorts

In each cohort, both extratumoral and intratumoral density distributions of $CD3^+$ and $CD8^+$ T cells were compared with different NCS levels through Wilcoxon rank-sum test to assess the association between NCP and the immune infiltration, considering adjusted Benjamini-Hochberg p-values <0.05 as statistically significant. Overall (OS) and disease-free survival (DFS) were estimated by Kaplan-Meier curves and Cox proportional hazard models, considering the two cohorts both separately and joint stratifying by cohort. Age, gender, etiology, alpha-fetoprotein tumor marker, stage, Child-Pugh staging system, Barcelona Clinic Liver Cancer Staging System and multinodularity were considered as confounders in the models, selecting them with a step-down procedure based on a χ^2 test for goodness of fit: all the available confounders were first included in the full model considering main effects only, and then sequentially removed if their removal did not result in a significant change of the estimates. The significance of the final model was evaluated in terms of both log-rank and likelihood ratio tests for the significance of the coefficient associated with the variable of interest in the model, used to derive the corresponding hazard ratios (HRs) and confidence intervals (CIs). Both NCS and the single receptors (RIPK1, RIPK3, and MLKL), as well as the distributions of $CD3^+$ and $CD8^+$ T cells densities, were evaluated separately. For T cell densities, discretized values were considered using quantiles and dividing the corresponding extratumoral/intratumoral distributions into three uniformly distributed levels at low, intermediate and high densities to easily compare them with NCS. Analyses were performed with R (V.4.0.3, https://www.R-project.org/).

RESULTS

Genes involved in necroptosis mainly associated with inferred $CD8^+$ T cells infiltration

No statistically significant differences were observed for demographic and pathological data of the 70+70 TCGA-LIHC patients between low and high infiltration of $CD8^+$ T cells (see table S2 and figure S3 in online supplemental file 1); therefore, no other confounding factors were added to the logistic models testing for the associations with the immune infiltration. The univariate logistic regression selected 10 genes from the necroptosis pathway, including both *RIPK3* and *MLKL*, as significantly associated to $CD8^+$ T cell infiltration (figure 1B and red nodes in figure 1C), which showed higher expression in samples at high $CD8^+$ T cell infiltration. Additional genes

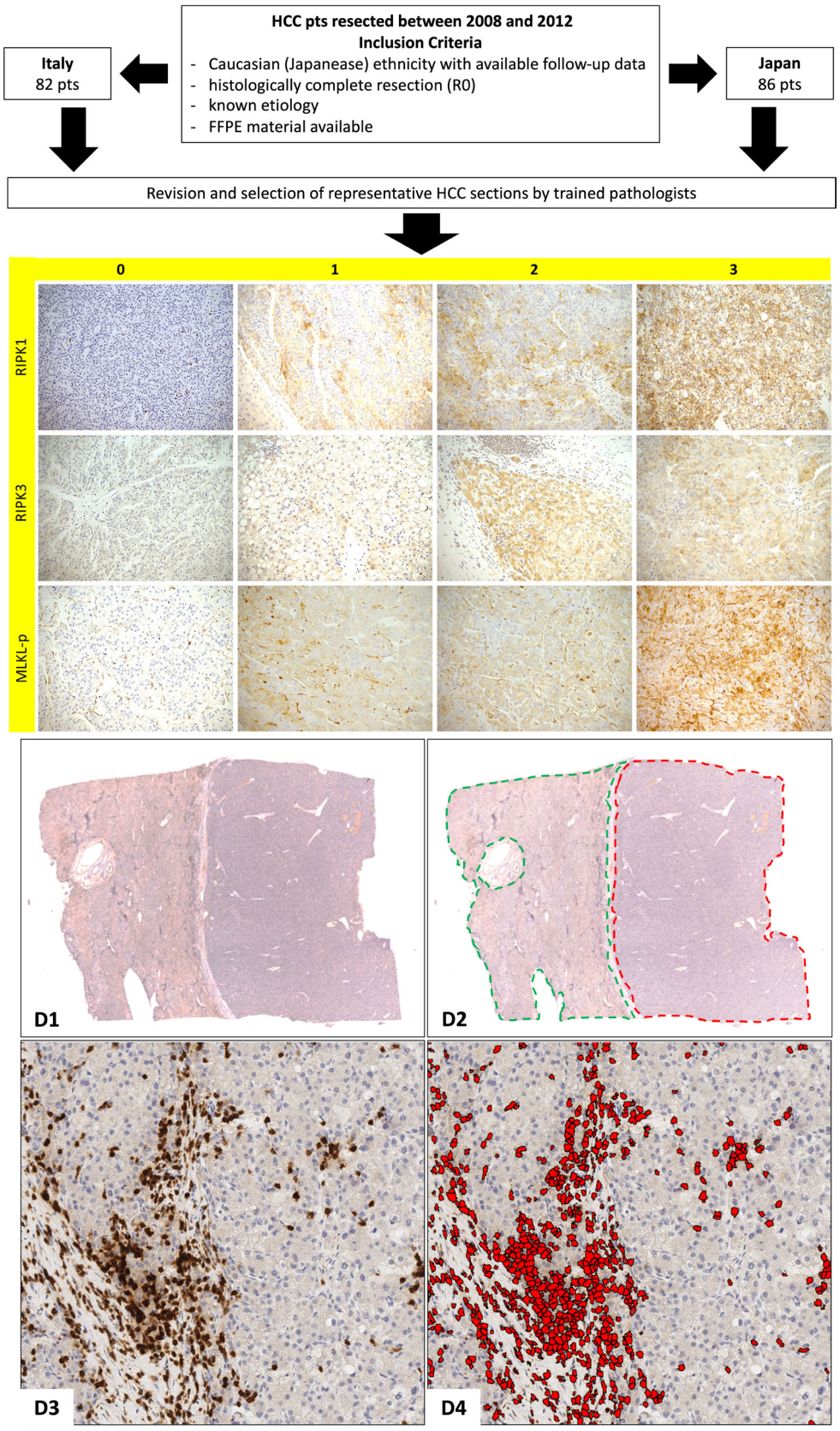

Figure 2 Graphical pathological workflow. Upper boxes show the selection criteria for both the cohorts and the representative immunohistochemistry stains of scores for each marker (original magnifications 200×). In the lower boxes, an example of automatic assessing of CD3-positive cells is shown: first, the digitized whole slide section was opened (D1) and both tumor tissue (red line) and non-tumor tissue (green line) were manually annotated (D2). After tissue annotation, automatic CD3-positive cells detection was performed with Visiopharm software, V.4.5.6.5 (Visiopharm, Hoersholm, Denmark): D4 the same area showed in D3 after positive cells recognition. Abbreviations: HCC, hepatocellular carcinoma.

Table 2 Demographic, pathological, immunohistochemical and imaging data of the patients from Italian and Japanese cohorts

Group	Japan (n=86)	Italy (n=82)	P value
Age (years)			
Mean (SD)	69 (8.5)	66 (9.9)	0.47
Sex, % (n)			
Female	28 (24)	20 (16)	0.27
Male	72 (62)	80 (66)	
Etiology, % (n)			
Non-viral	24 (21)	38 (31)	0.087
Viral (HBV/HCV)	76 (65)	62 (51)	
AlphaFP (ng/mL), n (%)			
<400	86 (74)	91 (75)	0.39
≥400	14 (12)	8.5 (7)	
CHILD, % (n)			
A	90 (77)	79 (65)	0.1
B/C	10 (9)	21 (17)	
BCLC, % (n)			
0/A	37 (32)	39 (32)	0.93
B/C	63 (54)	61 (50)	
Portal thrombosis, % (n)			
Absent	37 (32)	94 (77)	<0.001
Present	63 (54)	6.1 (5)	
Stage, % (n)			
I–II	57 (49)	79 (65)	0.0034
III–IV	43 (37)	21 (17)	
Maximun dimension (mm)			
Mean (SD)	31 (21)	49 (30)	<0.001
Multinodularity, % (n)			
Absent	88 (76)	87 (71)	0.91
Present	12 (10)	13 (11)	
$CD3^+$ T cells density (cells/mm^2)			
Mean (SD)	657 (684)	567 (524)	0.31
$CD8^+$ T cells density (cells/mm^2)			
Mean (SD)	356 (384)	318 (445)	0.18
NCS, % (n)			
Low	23 (20)	27 (22)	0.27
Intermediate	49 (42)	54 (44)	
High	28 (24)	20 (16)	
Survival, % (n)			
Alive	65 (56)	35 (29)	<0.001
Dead	35 (30)	65 (53)	
Survival time (months)			
Mean (SD)	52 (19)	40 (25)	<0.001
Recurrence, % (n)			
Absent	21 (18)	12 (10)	0.46
Present	72 (62)	63 (52)	

Continued

Table 2 Continued

Group	Japan (n=86)	Italy (n=82)	P value
Missing	7 (6)	24 (20)	
Recurrence time (months)			
Mean (SD)	33 (22)	26 (23)	0.022
Valid (missing)	80 (6)	62 (20)	

P-values correspond to Kolmogorov-Smirnov and χ^2 tests for numerical and nominal data, respectively.
AlphaFP, alpha-fetoprotein tumor marker; BCLC, Barcelona Clinic Liver Cancer Staging System; CHILD, Child-Pugh Staging System; HBV, hepatitis B virus; HCV, hepatitis C virus; NCS, necroptosis core score.

were then selected through the multivariate analysis that might interact with the process of immune infiltration (blue nodes in figure 1C). As expected, the complex *RIPK3/MLKL* resulted enhanced at high $CD8^+$ infiltration and the interactions *RIPK1–>RIPK3*, *RIPK3–>MLKL* and *RIPK1–>RIPK3–>MLKL* were found eight times among the 19 paths (red edges in figure 1C) resulted statistically significant from the multivariate analysis (see table S3 in online supplemental file 1). Looking at the other selected genes/paths, the association between the complex *RIPK1/RIPK3/MLKL* and the immune infiltration seems to be mainly activated by interferons (*IFNG*, *IFNGR1*), which are known to regulate innate and acquired immunity, resistance to viral infections, and cell survival/death (figure 1C). Specifically, *IFNGR1* activates the JAK-STAT signaling pathway, leading to the transcription of downstream genes including those related with the necrosome formation. In addition, *ZBP1*, a Z-DNA-binding protein that can be induced by IFNs, was selected and found to increase its expression in samples at high $CD8^+$ T cell infiltration. Like *RIPK1* and *RIPK3*, *ZBP1* is a RHIM (RIP homotypic interaction motif) domain-containing protein, implying its potential role in associating with *RIPK1* and *RIPK3* to participate in necroptosis.[20]

Despite *CASP8* did not show a statistically significant underexpression in samples at high $CD8^+$ T cell infiltration, there is an overexpression of *CASP1*, which is known to be activated by inflammasomes and promotes

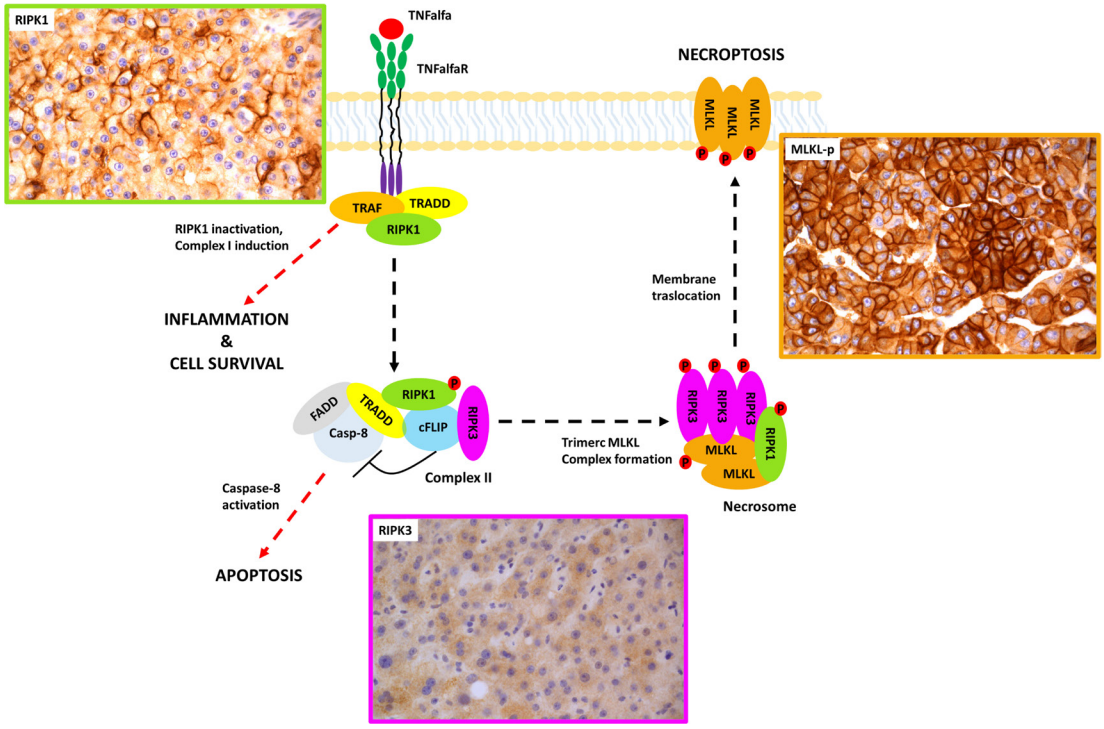

Figure 3 General overview of the main factors involved in the necroptosis machinery with representative stains of each marker investigated in this study. RIPK1 is firstly involved after necroptosis activation (through TNF-alpha in this case). As shown by immunohistochemistry, RIPK1 explains its function mainly in the cellular membrane and into the cytoplasm (green box). RIPK3 is then involved and activated through a phosphorylation process in the cytoplasm (purple box). Finally, MLKL interacts with the complex II (driven by RIPK3) and forms the so-called necrosome. After activation through phosphorylation, MLKL-p migrates to the membrane where it forms a trimeric pore carrying out the necroptosis. Immunohistochemistry for MLKL-p results in a strong membrane and cytoplasmic reaction (orange box). Original magnification of representative cases of HCC: 200×. Abbreviations: HCC, hepatocellular carcinoma

both the maturation and the secretion of proinflammatory cytokines. This process is also confirmed by the coactivation of *NLRP3* that drives the inflammasome activity and the proinflammatory cytokine *ILB1*. Finally, interactions between *MLKL* and the endosomal sorting complex required for transport-III (including *CHMP1A*, *CHMP1B*, *CHMP3*, *CHMP4A* and *CHMP4C*), which plays a key role in repairing the damaged plasma membranes, were selected.

Demographic data

Clinicopathological data are resumed in table 2. Comparing the two cohorts, Japanese cohort showed more cases with advanced tumor stage, that is, 43% (37 patients) with stage III or IV, and portal thrombosis (63%, 54 patients) than Italian cohort, that is, 21% (17 patients) with stage III or IV, and 6.1% (5 cases) with portal thrombosis.

IHC and fluorescence imaging

Scores of each marker are listed in table S4 in online supplemental file 1. In the Japanese cohort, NCP markers combined as NCS resulted to low, intermediate and high in 23%, 49% and 28% of the patients, while 27%, 54% and 20% of the patients in the Italian cohort, respectively. No significant differences were observed between the cohorts in terms of NCS. Considering each marker separately, Japanese patients showed more RIPK1 positive (ie, score >0) immunostaining (p=0.0017), while no significant differences were observed for both RIPK3 and MLKL-p.

TILs showed a mean density of 612.93 cells/mm^2 while infiltrating CD8$^+$ T cells showed a mean density of 337.45 cells/mm^2. TILs and intratumor CD8$^+$ T cells were correlated (Pearson's correlation 0.784; p value <0.001), and no significant differences were observed between the cohorts (table 2).

Considering multiplex fluorescent microscopy, RIPK1, RIPK3, and MLKL-p resulted strongly colocalized in the same tumor cells (example shown in figure 4; Pearson's correlation: 0.86–0.98 for MLKL vs RIPK1 and 0.89–0.98 for RIPK3 vs RIPK1). Morphology of necroptotic cells showed an enlargement (DIC imaging) and disappearance of the nuclei (DAPI signal) in tumor cells colocalizing RIPK1, RIPK3, and MLKL-p.

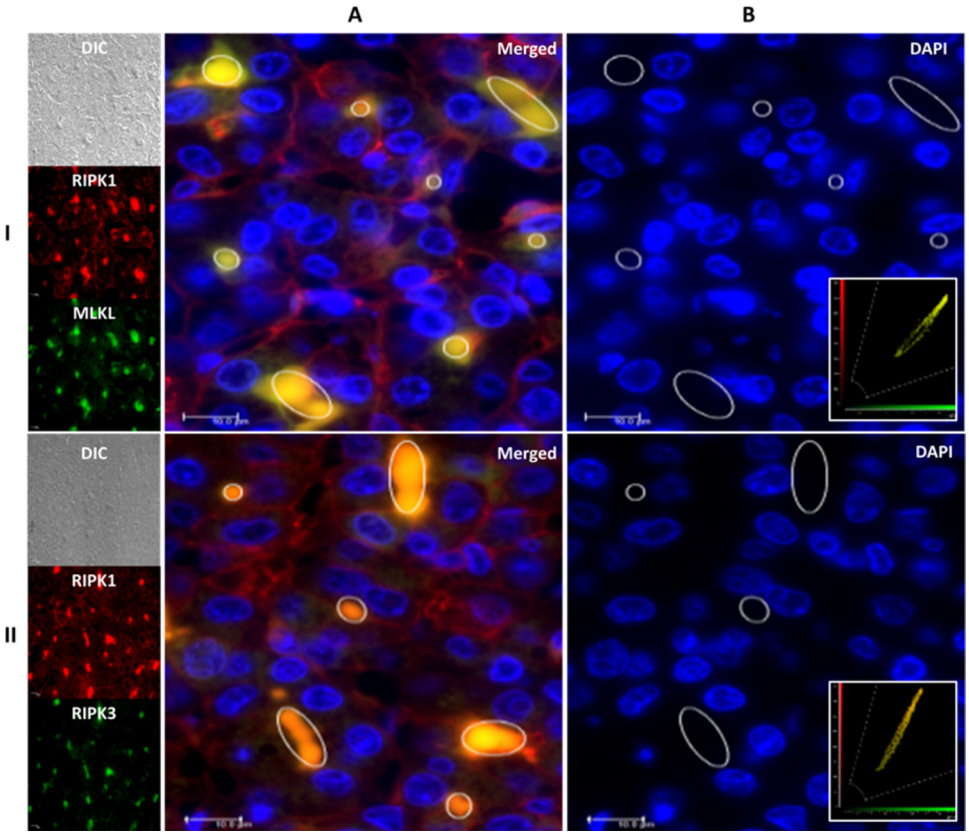

Figure 4 Expression of MLKL, RIPK3 and RIPK1 staining in HCC tissue sections analyzed with multiplex imaging. Column A showed the merged picture of individual stains shown in the small box of the left panel. Cell morphology was visualized by differential interference contrast (DIC) (grayscale image in the left panel). Line I: antihuman MLKL (green) and antihuman RIPK1 (red). Line II: antihuman RIPK3 (green) and antihuman RIPK1 (red). Nuclei were labeled with Hoechst 33258 (blue fluorescence). The circles in the merged images highlight necroptotic cells coexpressing RIPK1, RIPK3 and MLKL-p (yellow); note the absence of the nucleus in correspondence of the cells coexpressing RIPK1, RIPK3 and MLKL-p (circles in column B). Representatives' cytofluorograms of colocalization analysis in the bottom right of line I and II show the intensity relationships between the two channels from a representative region of interest (ROI). Images were acquired by a fluorescence microscope Leica DMI6000CS, 63×/1.4 oil immersion objective, using a DFC365FX camera and LAS-AF 3.1.1 software. Scale bar 10 µm.

Association of NCS with CD3+ and CD8+ T cells infiltration

Increased levels of NCS showed statistically significant association with higher $CD3^+$ and $CD8^+$ T cells intratumoral, but not extratumoral, infiltration in both cohorts (figure 5A). Considering the three receptors independently, this association was not always found preserved for all the receptors and the cohorts (figure S4A in online supplemental file 1). However, considering the densities of $CD3^+$ and $CD8^+$ dichotomized by their median value, $CD8^+$ was found significantly associated with all the receptors in both cohorts, while $CD3^+$ showed significant associations with MLKL and RIPK1 in the Italian cohort and with MLKL and RIPK3 in the Japanese cohort (figure S4B in online supplemental file 1).

Prognostic relevance of NCS in hepatocarcinoma

Considering survival and relapse at 5 years of follow-up, we found significant differences between Italian and Japanese cohorts in terms of OS and, partially, DFS (table 2 and figure S5 in online supplemental file 1, with Kaplan-Meier p values 1e-04 in OS and 0.054 in DFS). Therefore, the prognostic relevance of NCS in OS and DFS was assessed both in the two cohorts separately and in the joint dataset stratifying by cohort. NCS was found significantly correlated with OS both when the cohorts were considered separately (figure 5B) and when they were joined (figure S6 in online supplemental file 1), while for DFS the significance was observed only in the Italian cohort and in the joint dataset (results from Cox models in table 3 and table S5 in online supplemental file 1). Considering the three receptors separately, RIPK3 showed significant association with OS both when the cohorts were considered separately and when they were joined, while both RIPK1 and MLKL showed significant association in the Italian, but not Japanese, cohort and in the joint dataset (table S6 in online supplemental file 1). In terms of DFS, only RIPK1 was significantly associated in the Italian, but not Japanese, cohort and when the cohorts were joined. Focusing on the immune infiltration, only intratumoral $CD8^+$ T cell infiltration showed significant association with OS in the Italian cohort and in the joint dataset (figure S7 in online supplemental file 1), with results in the Japanese cohort extremely close to the significance threshold (log-rank test p value=0.0205 and likelihood ratio test p value=0.0517, table S7 in online supplemental file 1).

Finally, we checked on the clinical data from TCGA-LIHC whether the results observed for OS in our cohorts are also confirmed at mRNA level by defining a combined score of the three receptors from RNA-seq data, as done for NCS. Specifically, we discretized the gene expression of each receptor into four levels, considering the quantiles with thresholds equal to those used to quantify the expression of RIPK1, RIPK3 and MLKL in our cohorts, that is, 0 (<5%); 1+ (5%–25%); 2+ (25%–65%); and 3+ (>65%), and then assembled them into a score named as NCSrna in the following. Since no statistically significant differences in terms of ethnicity of the patients were observed (p value 0.23, figure S8 in online supplemental file 1), the whole dataset (279 samples with available information for OS) was analyzed to evaluate the prognostic relevance of NCSrna. For the Cox models, clinical factors reported in table 1 were considered as potential confounders, excluding those reporting >5% of the samples with missing values and selecting them according to the same step-down procedure described in Materials and methods for our cohorts. Survival analysis was applied to NCSrna, to the three receptors separately and to the $CD8^+$ T cell infiltration. For this latter, we kept the previous classification of 140 patients at low and high immune infiltration classifying the other patients at an intermediate infiltration level. Results confirmed the significant associations found among NCP, $CD8^+$ T cell infiltration, and OS (figure S9 and table S8 in online supplemental file 1). Considering the three receptors independently, only RIPK3 was statistically significant for prognosis alone (table S8 in online supplemental file 1).

DISCUSSION

The links between the cancer features and the immune TME is to date a well-accepted paradigm; however, the factors driving TME composition and functions, as well as TILs recruitments are still largely unknown.[21] Within this context, NCP could play a role as a possible immune regulator.[22] Immunogenicity of NCP in tissues has been extensively demonstrated; however, its immunological and clinical impact in cancer is still poorly investigated. So far, both in vitro and in vivo experimental studies showed that dendritic cells and other antigen presenting cells (APCs) may be activated by the DAMPs released by the necroptotic tumor cells that, in turn, boost a specific antitumoral immune response through cross-priming of cytotoxic $CD8^+$ T cells.[23 24 25] This model may explain, at least in part, the hypothesis that NCP suppression in cancer cells should reduce the number of tumor-derived epitopes released and identifiable by APC, suggesting NCP downregulation as a possible immune escape strategy. This observation is consistent with studies showing a correlation between the downregulation of *RIPK1*, *RIPK3*, or *MLKL* with poor prognosis in several cancers.[26] However, not all of them necessarily show NCP downregulation: correlation between upregulated NCP factors and worse prognosis has been previously found in glioblastoma and lung cancer.[26] The ambiguous role played by NCP in cancer biology was also highlighted by another study that showed how NCP occurring in tumor-associated vessels should be implicated in favoring metastatic spreading.[27]

In this study, for the first time, 371 cases of patients with HCC from TCGA repository were used to perform a comprehensive analysis on 163 genes involved in the necroptotic pathway using annotations from KEGG database.[14] In silico analysis revealed that the high expression of the complex RIPK3/MLKL and its combination with RIPK1 was associated with an increased level of

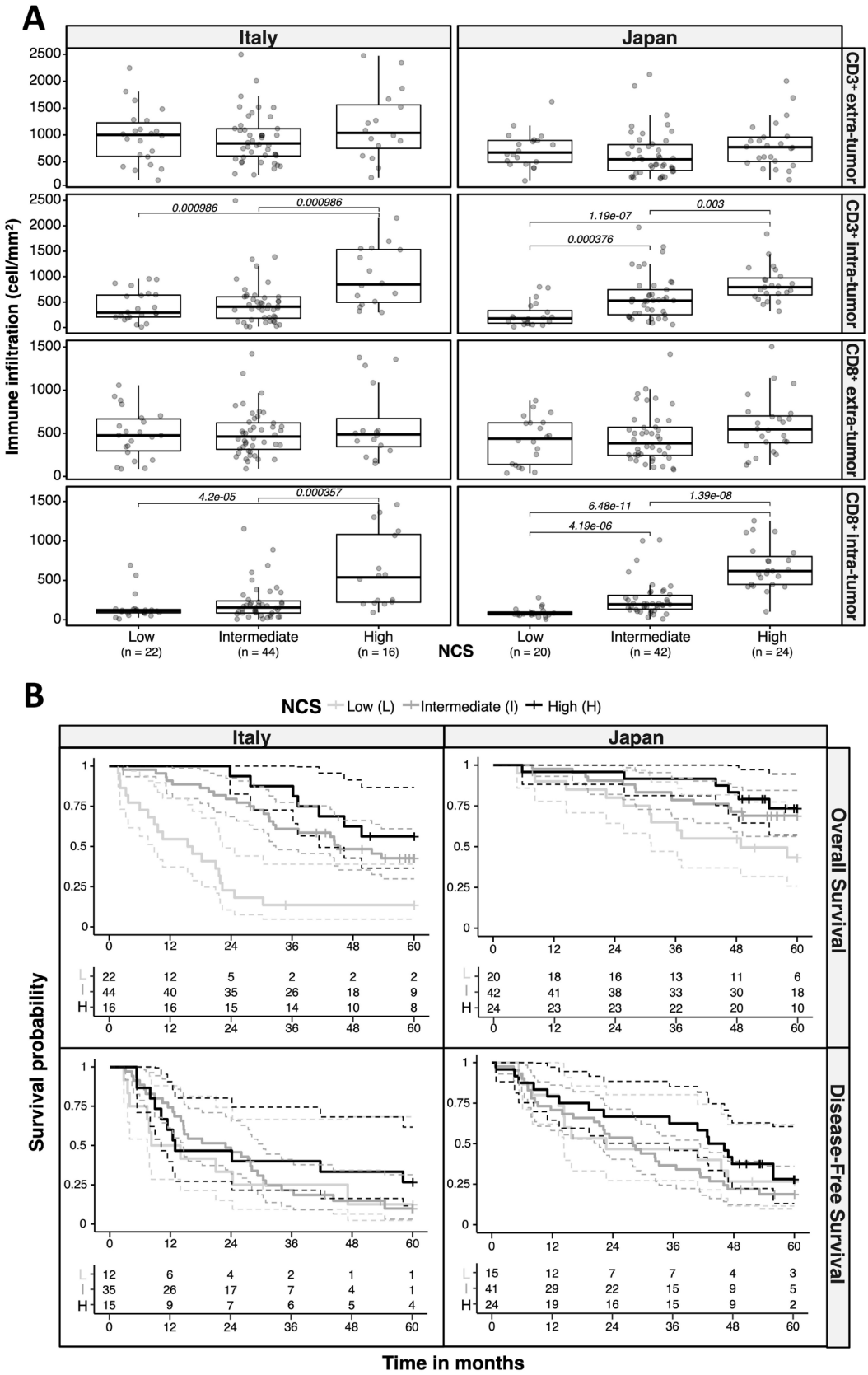

Figure 5 Evaluation of the immunological role and the prognostic value of NCS in both Japanese and Italian cohorts, separately. (A) Associations between the NCS and the intratumoral/extratumoral infiltration of $CD3^+$ and $CD8^+$. The boxplots show the density levels of immune infiltration according to the three levels assigned to NCS (low, intermediate, and high). Benjamini-Hochberg adjusted p-values for pairwise comparisons performed through Wilcoxon's rank-sum test are reported for significant comparisons. (B) Kaplan-Meier curves for both overall and disease-free 5-year survival. For each box, the curves represent the three levels assigned to NCS (low, intermediate, and high). Abbreviations: NCS, necroptosis core score.

Table 3 Cox regression models of NCS for both overall survival (OS) and disease-free survival (DFS) in Italian and Japanese cohorts

Cohort	Survival	Log-rank test	Likelihood ratio test	HR	95% CI	Confounders
Italian	OS	4.52e-08	6.63e-06	0.313	(0.189 to 0.518)	AlphaFP, CHILD, multinodularity
Italian	DFS	0.0261	0.285	0.791	(0.515 to 1.22)	Multinodularity
Japanese	OS	0.0091	0.0203	0.544	(0.325 to 0.91)	Age
Japanese	DFS	0.00837	0.0778	0.704	(0.476 to 1.04)	BCLC

The models are evaluated in terms of: (1) p-value from log-rank test assessing the fit performance of the whole model including both NCS and confounders; (2) p-value from likelihood ratio test assessing the statistical significance of the specific coefficient estimated for NCS in the model, used to derive the corresponding HR with the related 95% CI. The confounders reported in the last column are those selected for the final model after the step-down selection procedure described in the Materials and methods section.
AlphaFP, alpha-fetoprotein tumor marker; BCLC, Barcelona Clinic Liver Cancer Staging System; CHILD, Child-Pugh Staging System; NCS, necroptosis core score.

$CD8^+$ T cells signature in HCC (figure 1). Therefore, we used two additional cohorts involving 168 HCC patients recruited in Italy (82) and Japan (86) to test our preliminary observation, extending the analysis to a more general T-lymphocyte population CD3-positive. In both cohorts, an increasing level of immunoreaction score of RIPK1, RIPK3 and MLKL-p resulted in an increasing level of intratumoral density of $CD3^+$ and $CD8^+$ T-lymphocytes (figure 5A and figure S4 in online supplemental file 1), enforcing the immunogenic role of NCP in cancer,[28] as also previously shown in breast cancer[29] and, recently, in cholangiocarcinoma.[30]

NCS, as well as tumor-infiltrating $CD8^+$ T cells, showed also prognostic relevance in terms of OS, while TILs were not found associated with a worse prognosis in both Italian and Japanese cohorts (figure 5B with table 3 and figure S6 with table S5 in online supplemental file 1 for NCS; figure S7 with table S7 in online supplemental file 1 for $CD8^+$ T cells and TILs). These results were also confirmed in TCGA-LIHC data considering NCS as a combined mRNA expression score of the three receptors and the inferred $CD8^+$ T cells infiltration from RNA-seq data through deconvolution approaches (figure S9 and table S8 in online supplemental file 1). Despite infiltrating $CD8^+$ T cells have been reported as good prognostic markers in HCC,[31] a different impact on the prognosis has been observed according to specific cell types, enforcing the evidence that the dynamic evolution in terms of cell composition may show opposite effects on tumor biology, promoting or blocking tumor evolution.[32 33] Several aspects could explain these differences: (1) our analysis did not take into account the spatial distribution of T cell infiltrates: location of immune infiltrates inside the tumor core and the invasive front have been described as independent predictors of clinical outcome,[34 35]; (2) it is possible that in our cohorts TILs should be principally composed by subsets of T cells including Treg and Th-17 cells linked to immune suppression and cancer progression in several cancers including HCC[33 36]; (3) immune escape mechanisms and T cell exhaustion phenomena may predominate blocking TILs-mediated tumor suppression[37]; (4) the lack of an accepted consensus to normalize TILs scoring in HCC across different institutions and also different aetiologies might play a role to explain these differences.

In our cohorts, all the three receptors used to define NCS were found significantly associated with OS in the stratified Cox model, while when the two cohorts were analyzed separately, only RIPK3 was able to preserve a significant association with OS in both Italian and Japanese cohorts, while RIPK1 and MLKL-p were found significantly correlated with worse prognosis only in the Italian cohort (table S6 in online supplemental file 1). These differences might also be due to the limited number of patients available by considering each cohort separately. However, the prognostic effect of NCS observed in our study highlights its real utility within clinical management and the need to be further investigated in future studies on larger cohorts. NCS assessment could be further improved by automatic assessment through image analysis tools, which may provide a more objective and standardizable results. In support of these observations, the higher prognostic relevance of RIPK3 in HCC with respect to the other two receptors was also confirmed at RNA level in the TCGA-LIHC cohort (table S8 in online supplemental file 1). Although hepatocytes clearly express *MLKL* at basal conditions, which in this study showed the strongest association with $CD8^+$ and TILs infiltration (figure S4 in online supplemental file 1), the presence of RIPK3 in liver cells has been controversial, and it might only be induced in certain disease conditions of the liver.[38] Recently, Afonso and colleagues[39] showed that hepatic RIPK3 correlates with NAFLD severity in humans and mice, playing a key role in managing liver metabolism, damage, inflammation, fibrosis and carcinogenesis. However, results found in RIPK1 showed some differences with respect to RIPK3 and MLKL. In our survival analysis, RIPK1 was the only receptor showing some prognostic relevance also in terms of DFS, while in silico analysis showed that *RIPK1* did not result significantly active alone with respect to the immune infiltration, but in combination with other genes (mainly *STATs* and *RIPK3*). In addition, both CYLD, the RIPK1-deubiquitinating enzyme cylindromatosis required for optimal necroptotic responses, and

TNFAIP3, promoting RIPK1 ubiquitination suppressing necroptosis by deubiquitinating RIPK3,[40] were selected as significantly associated with immune infiltration in HCC (figure 1). However, *TNFAIP3* was selected only when combined with other genes (table S3 in online supplemental file 1). RIPK1 is recognized as a protein with 'two faces': one promoting cell survival through its scaffolding properties and one favoring cell death through its kinase activity,[41 42] Van *et al*[43] showed that RIPK1 can either prevent or, combined with NF-κB, drive hepatocyte apoptosis, chronic liver disease, and cancer according to the presence or absence of the NF-κB essential modulator. Therefore, considering the crosstalk of RIPK1 in apoptosis, necroptosis, and NF-κB pathways, the inhibition of RIPK3 kinase activity seems to be a more specific therapeutic target for necroptosis in HCC. Finally, our in silico analysis highlighted other potential genes and interactions that might enhance the immune response in HCC and which can be considered for future validations (figure 1 and table S3 in online supplemental file 1). For example, in support of our findings, interferons (IFNs) were recently found to induce necroptosis in RelA-deficient cells, suggesting that NF-κB blocks IFN-induced necroptosis in wild-type cells,[44] while Baik *et al*[45] found that *ZBP1* expression is dramatically elevated in necrotic breast tumors, and it mediates necroptosis during the tumor development by inducing the activation of MLKL.

In conclusion, our results confirmed the immunogenetic properties of NCP in human HCC, showing that TILs and $CD8^+$ T cells accumulate in tumors with higher expression of NCP genes. These results suggest the importance of further studies to better assess the composition, the functional and evolutionary features, as well as possible checkpoints targeting the immune environment associated with a necroptotic signature in order to explore new diagnostic and therapeutic scenarios.

Author affiliations
[1]Department of Medicine (DIMED), University of Padova, Padova, Italy
[2]Department of Pathology, Angelo Hospital, Mestre, Italy
[3]Department of Medical Sciences, University of Torino, Torino, Italy
[4]Department of Pathology, Padova University Hospital, Padova, Italy
[5]Department of Pathology, Azienda ULSS2 Marca Trevigiana, Treviso, Italy
[6]Department of Diagnostic Pathology, Kurume University Hospital, Kurume, Japan
[7]Department of Medicine, General Internal Medicine and Thrombotic and Hemorrhagic Diseases Unit, University of Padova, Padova, Italy
[8]Department of Statistical Sciences, University of Padova, Padova, Italy
[9]Department of Surgery, Oncology and Gastroenterology, University of Padova, Padova, Italy
[10]II Surgery Unit, Regional Hospital Treviso, Treviso, Italy
[11]Department of Pathology, Kurume University School of Medicine, Kurume, Japan

Acknowledgements TS received funding specifically appointed to Department of Medical Sciences of University of Torino from the Italian Ministry for Education, University and Research (Ministero dell'Istruzione, dell'Università e della Ricerca—MIUR) under the programme 'Dipartimenti di Eccellenza 2018–2022' Project code D15D18000410001; GC and DS were supported by PRIN2017 (20178S4EK9), Progetti di Rilevante Interesse Nazionale, MIUR. We would like to thank VG for the technical support.

Contributors Conceptualization: LN and TS. Experimental design: LN, RC, VM, JA, AK and YN. Bioinformatics: TS. Immunofluorescence: CMR and PS. Data analysis: LN, TS, RC and VM. Statistical analysis: TS, DS and GC. Writing: LN and TS. Supervision: MG, AF, GZ and HY. Guarantor: AF.

Competing interests None declared.

Patient consent for publication Not applicable.

Provenance and peer review Not commissioned; externally peer reviewed.

Data availability statement Data are available on reasonable request.

ORCID iDs
Lorenzo Nicolè http://orcid.org/0000-0001-8126-9674
Tiziana Sanavia http://orcid.org/0000-0003-3288-0631

REFERENCES

1 Bray F, Ferlay J, Soerjomataram I, *et al*. Global cancer statistics 2018: GLOBOCAN estimates of incidence and mortality worldwide for 36 cancers in 185 countries. *CA Cancer J Clin* 2018;68:394–424.
2 Villanueva A. Hepatocellular carcinoma. *N Engl J Med* 2019;380:1450–62.
3 Fong ZV, Tanabe KK. The clinical management of hepatocellular carcinoma in the United States, Europe, and Asia: a comprehensive and evidence-based comparison and review. *Cancer* 2014;120:2824–38.
4 Fridman WH, Zitvogel L, Sautès-Fridman C, *et al*. The immune contexture in cancer prognosis and treatment. *Nat Rev Clin Oncol* 2017;14:717–34.
5 Newell EW, Becht E. High-dimensional profiling of tumor-specific immune responses: asking T cells about what they "see" in cancer. *Cancer Immunol Res* 2018;6:2–9.
6 Gnjatic S, Bronte V, Brunet LR, *et al*. Identifying baseline immune-related biomarkers to predict clinical outcome of immunotherapy. *J Immunother Cancer* 2017;5:44.
7 Gabrielson A, Wu Y, Wang H, *et al*. Intratumoral CD3 and CD8 T-cell densities associated with relapse-free survival in HCC. *Cancer Immunol Res* 2016;4:419–30.
8 Sun C, Xu J, Song J, *et al*. The predictive value of centre tumour $CD8^+$ T cells in patients with hepatocellular carcinoma: comparison with immunoscore. *Oncotarget* 2015;6:35602–15.
9 Garg AD, Agostinis P. Cell death and immunity in cancer: from danger signals to mimicry of pathogen defense responses. *Immunol Rev* 2017;280:126–48.
10 Galluzzi L, Vitale I, Warren S, *et al*. Consensus guidelines for the definition, detection and interpretation of immunogenic cell death. *J Immunother Cancer* 2020;8:e000337.
11 Tang D, Kang R, Berghe TV. The molecular machinery of regulated cell death. *Cell Res* 2019.
12 Meng M-B, Wang H-H, Cui Y-L, *et al*. Necroptosis in tumorigenesis, activation of anti-tumor immunity, and cancer therapy. *Oncotarget* 2016;7:57391–413.
13 Cancer Genome Atlas Research Network. Cancer genome atlas research network. *Cell* 2017;169:1327–41.
14 Kanehisa M, Goto S, Sato Y, *et al*. Kegg for integration and interpretation of large-scale molecular data sets. *Nucleic Acids Res* 2012;40:D109–14.
15 Aran D, Sirota M, Butte AJ. Systematic pan-cancer analysis of tumour purity. *Nat Commun* 2015;6:8971.
16 Who Press. *Who classification of tumours editorial board, digestive system tumours*, 2019.
17 Sauerbrei W, Taube SE, McShane LM, *et al*. Reporting recommendations for tumor marker prognostic studies (REMARK): an abridged explanation and elaboration. *Cancer Inst* 2018;110:803–11.

18 Nicolè L, Cappellesso R, Sanavia T, *et al*. Mir-21 over-expression and programmed cell death 4 down-regulation features malignant pleural mesothelioma. *Oncotarget* 2018;9:17300–8.
19 Cappellesso R, Nicolè L, Zanco F, *et al*. Synchronous nodal metastatic risk in screening detected and endoscopically removed pT1 colorectal cancers. *Pathol Res Pract* 2020;216:152966.
20 Kuriakose T, Kanneganti T-D. Zbp1: innate sensor regulating cell death and inflammation. *Trends Immunol* 2018;39:123–34.
21 Mantovani A, Allavena P, Sica A, *et al*. Cancer-related inflammation. *Nature* 2008;454:436–44.
22 Snyder AG, Hubbard NW, Messmer MN, *et al*. Intratumoral activation of the necroptotic pathway components RIPK1 and RIPK3 potentiates antitumor immunity. *Sci Immunol* 2019;4:aaw2004.
23 Aaes TL, Kaczmarek A, Delvaeye T, *et al*. Vaccination with Necroptotic cancer cells induces efficient anti-tumor immunity. *Cell Rep* 2016;15:274–87.
24 Kaczmarek A, Vandenabeele P, Krysko DV. Necroptosis: the release of damage-associated molecular patterns and its physiological relevance. *Immunity* 2013;38:209–23.
25 Qin X, Ma D, Tan Y-X, *et al*. The role of necroptosis in cancer: a double-edged sword? *Biochim Biophys Acta Rev Cancer* 2019;1871:259–66.
26 Gong Y, Fan Z, Luo G, *et al*. The role of necroptosis in cancer biology and therapy. *Mol Cancer* 2019;18:100.
27 Strilic B, Yang L, Albarrán-Juárez J, *et al*. Tumour-cell-induced endothelial cell necroptosis via death receptor 6 promotes metastasis. *Nature* 2016;536:215–8.
28 Gamrekelashvili J, Greten TF, Korangy F. Immunogenicity of necrotic cell death. *Cell Mol Life Sci* 2015;72:273–83.
29 Stoll G, Ma Y, Yang H, *et al*. Pro-necrotic molecules impact local immunosurveillance in human breast cancer. *Oncoimmunology* 2017;6:e1299302.
30 Lomphithak T, Akara-Amornthum P, Murakami K, *et al*. Tumor necroptosis is correlated with a favorable immune cell signature and programmed death-ligand 1 expression in cholangiocarcinoma. *Sci Rep* 2021;11:11743.
31 Xu X, Tan Y, Qian Y, *et al*. Clinicopathologic and prognostic significance of tumor-infiltrating CD8+ T cells in patients with hepatocellular carcinoma: a meta-analysis. *Medicine* 2019;98:e13923.
32 Yang L, Lin PC. Mechanisms that drive inflammatory tumor microenvironment, tumor heterogeneity, and metastatic progression. *Semin Cancer Biol* 2017;47:185–95.
33 Ding W, Xu X, Qian Y, *et al*. Prognostic value of tumor-infiltrating lymphocytes in hepatocellular carcinoma: a meta-analysis. *Medicine* 2018;97:e13301.
34 Saltz J, Gupta R, Hou L, *et al*. Spatial organization and molecular correlation of tumor-infiltrating lymphocytes using deep learning on pathology images. *Cell Rep* 2018;23:181–93.
35 Petrizzo A, Buonaguro L. Application of the immunoscore as prognostic tool for hepatocellular carcinoma. *J Immunother Cancer* 2016;4:71.
36 Renaude E, Kroemer M, Loyon R, *et al*. The fate of Th17 cells is shaped by epigenetic modifications and remodeled by the tumor microenvironment. *Int J Mol Sci* 2020;21:1. doi:10.3390/ijms21051673
37 Itoh S, Yoshizumi T, Yugawa K, *et al*. Impact of immune response on outcomes in hepatocellular carcinoma: association with vascular formation. *Hepatology* 2020;72:1987–99.
38 Dara L, Liu Z-X, Kaplowitz N. Questions and controversies: the role of necroptosis in liver disease. *Cell Death Discov* 2016;2:16089.
39 Afonso MB, Rodrigues PM, Mateus-Pinheiro M, *et al*. RIPK3 acts as a lipid metabolism regulator contributing to inflammation and carcinogenesis in non-alcoholic fatty liver disease. *Gut* 2021;70:2359–72.
40 Feoktistova M, Leverkus M. Programmed necrosis and necroptosis signalling. *Febs J* 2015;282:19–31.
41 Weinlich R, Green DR. The two faces of receptor interacting protein kinase-1. *Mol Cell* 2014;56:469–80.
42 Blériot C, Lecuit M. Ripk1, a key survival factor for hepatocytes. *J Hepatol* 2017;66:1118–9.
43 Van T-M, Polykratis A, Straub BK, *et al*. Kinase-Independent functions of RIPK1 regulate hepatocyte survival and liver carcinogenesis. *J Clin Invest* 2017;127:2662–77.
44 Thapa RJ, Basagoudanavar SH, Nogusa S, *et al*. Nf-kappaB protects cells from gamma interferon-induced RIP1-dependent necroptosis. *Mol Cell Biol* 2011;31:2934–46.
45 Baik JY, Liu Z, Jiao D, *et al*. Zbp1 not RIPK1 mediates tumor necroptosis in breast cancer. *Nat Commun* 2021;12:2666.